HOMER

Workshop on Optical Metrology and Data Assimilation Applied to Aeroelastics

Delft, 22-23 Sept. 2021

Book of abstracts

HOMER

https://omda3.sciencesconf.org/

Workshop on Optical Metrology and Data Assimilation Applied to Aeroelastics
Sept. 22-23, 2021 | TU Delft, NL & Online

The HOMER workshop on Optical Metrology and Data Assimilation Applied to Aeroelastics aims at gathering experts of various horizons to share on novel diagnostic and analysis techniques for Aeroelastics and Fluid-Structure Interactions studies.

As part of the Holistic Optical Metrology for Aero-Elastic Research H2020 project, the Workshop offers the opportunity to the fluid and solid mechanics, biomechanics, physics and mathematics communities to exchange on innovative methodologies and recent results.

We wish all participants a fruitful workshop.

Ludovic Chatellier, Andrea Sciacchitano, Bas van Oudheusden

Workshop on Optical Metrology and Data Assimilation Applied to Aeroelastics
Sept. 22-23, 2021 | TU Delft, NL & Online

Table of contents

Optical Metrology

Workshop on Optical Metrology and Data Assimilation Applied to Aeroelastics
Sept. 22-23, 2021 | TU Delft, NL & Online

3D flow and deformation measurements of rigid and flexible wings under combined pitching and plunging motions using Lagrangian particle tracking

D. Schanz, R. Konrath, R. Geisler, A. O. Erdogdu, J.Agocs, A. Schröder
Institute of Aerodynamics and Flow Technology, German Aerospace Center (DLR), Göttingen, Germany

*daniel.schanz@dlr.de

Abstract

A dynamic test rig based on a hypocycloid gear (Huhn 2015) has been designed at DLR for underwater flapping wing applications (see Figure 1 a and b). Three NACA0012 wings with different flexibility, to be attached to the end plate, have been constructed (half span: 150 mm, chord: 50 mm). The wings perform a two-dimensional motion, i.e. within the x,z-plane, whereas the pitch axis is constantly pointing in the y-direction. Markers with approx. 0.5mm diameter were printed onto the wings with pseudo-random distribution to allow detection of the wing motion and deformation (see Figure 1 c and d).

The dynamic test rig was installed in the closed-circuit water tunnel at the Aerodynamic Institute (AIA) of the RWTH-Aachen tunnel to investigate the instantaneous aerodynamics of flapping wings (see Figure 1 f and g). The facility provides a 1.5 m wide and 1 m high test section and was operated at a free stream velocity of U = 0.44 m/s. A system of eight high-speed cameras (Phantom v2640, v1840 and T1340) were installed in two groups at both sides of the tunnel, providing a full view around the moving wings (see Figure 1 e and h). Illumination was realized using three high-power LED arrays, collimated by a 1000 mm lens and located beneath the tunnel. By using a passe-partout, a circular light volume with approx. 200 mm diameter was created, which was completely seen by all cameras (apart from the regions blocked by the wing for each camera). The spanwise extent of the measurements volume is approx. 220 mm. The water was seeded using 60 µm polyamide particles from *Orgasol*. The cameras and LEDs were operated at 2kHz repetition rate, yielding sequences of 12597 at the full camera resolution of 4 MPx. Various pitching and plunging motions at a frequency of 1.03 Hz were realized for all three wings, both with and without water flow.

The cameras were calibrated using a 3D calibration target from LaVision, which was translated by 150 mm in lateral direction. Volume-self-calibration (Wieneke 2007) and OTF calibration (Schanz et al. 2013) were applied. Figure 2 a) shows the positions of the cameras as given by the calibration in relation to the common volume, seen from above.

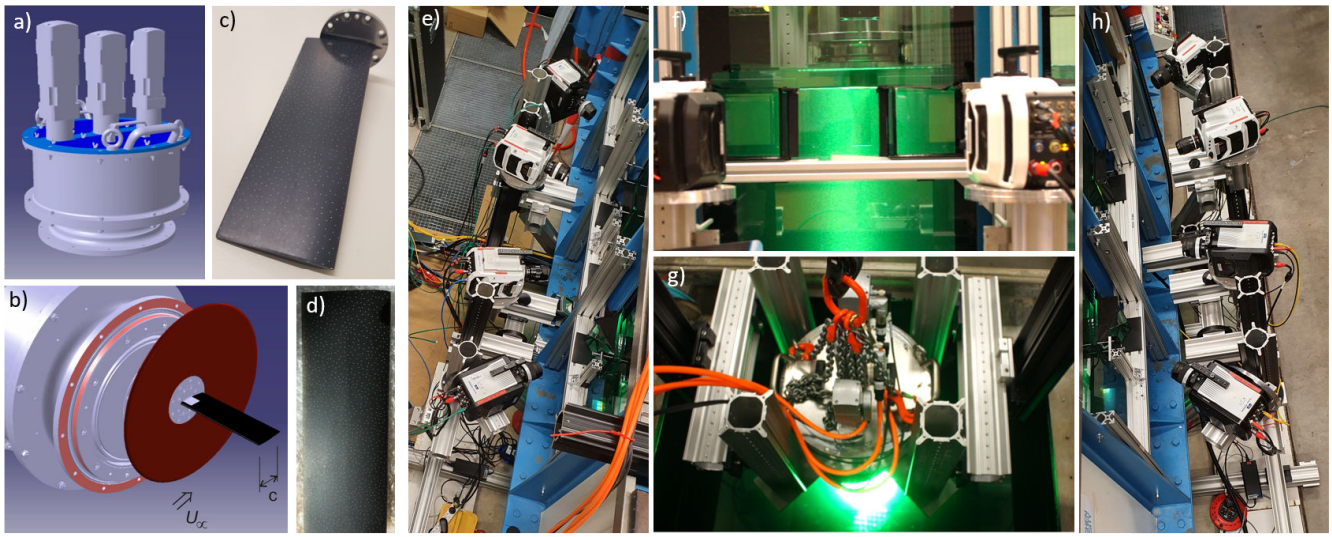

Figure 1: a) DLR dynamic test rig with three synchronized servo motors and gear box; b) half wing installed on end plate; c) rigid wing; d) flexible wing; e) and h) 4 cameras installed on each side of the water tunnel, forming a common camera system; f) side view of illuminated wing and particles; g) dynamic test rig installed on the top of the water tunnel

Both the particles, as well as the markers on the wing have been captured within the same images. The aim is to separately track both kinds of 3D points all around the model via Lagrangian particle tracking using the Shake-The-Box (STB) method (Schanz et al. 2016).

Evaluation starts with the detection of the wing. As a total of six cycles of the wing movement was captured in each run, a separation of the wing markers from the particle images is possible via the minimum images of the captured six instances of each phase. The tracking of the wing markers is then performed using STB on these minimum images, available for one full cycle. Figure 2-b shows tracked markers on a rigid wing, viewed from above, for several phases of a wing motion inspired by hovering humming birds without inflow (Masateru et al. 2017). A quick rotation of approx. 160 degree is followed by smaller-scale oscillations, while the wing is performing a plunging motion with 100 mm amplitude. Due to the difficult viewing conditions (in certain positions of the wing, many marker points are only visible in one or two cameras, due to geometry and reflections), not all markers can be tracked over the whole cycle. However, the total number of captured markers (600 - 800) is always enough to allow for a reliable detection of the wing. Figure 2 c) shows a side view of the wing markers for one time-step within the rotation movement.

The particle tracers are identified in a second process. The same time-resolved minimum images that were created for the tracking of the wing markers are subtracted from the original camera images in order to remove the marker images and most of the strong reflections on the end plate. The resulting images are used to reconstruct 3D positions using advance IPR processing (Wieneke 2013, Jahn et al. 2021). For the cases without water flow, Variable-timestep STB processing (Schanz et al. 2021) was applied due to the high dynamic velocity range. Time-separations of Δ_S = 10, Δ_S = 4 and Δ_S = 1 were used for a three-iteration reconstruction. Approximately 100.000 particles are tracked after the final iteration. Figure 2 d) shows an exemplary result from a single time-step of the same case as above. The particles are given as small circles with a velocity vector, color-coded with streamwise velocity, while the wing markers are depicted as black circles with velocity vectors, also color-coded with streamwise velocity. The quick rotational movement of the wing induces strong vortices in the fluid, where velocities up to 1.5 m/s are reached.

The evaluation is ongoing. The next task will be to fit a 3D FE-Model of the wing to the captured marker cloud, in order to fully describe the flexing of the wing. The fitted model, together with the particle velocity and acceleration data, will then be used in the FlowFit data assimilation method (Gesemann et al. 2016) for the extraction of time-resolved pressure and load distributions.

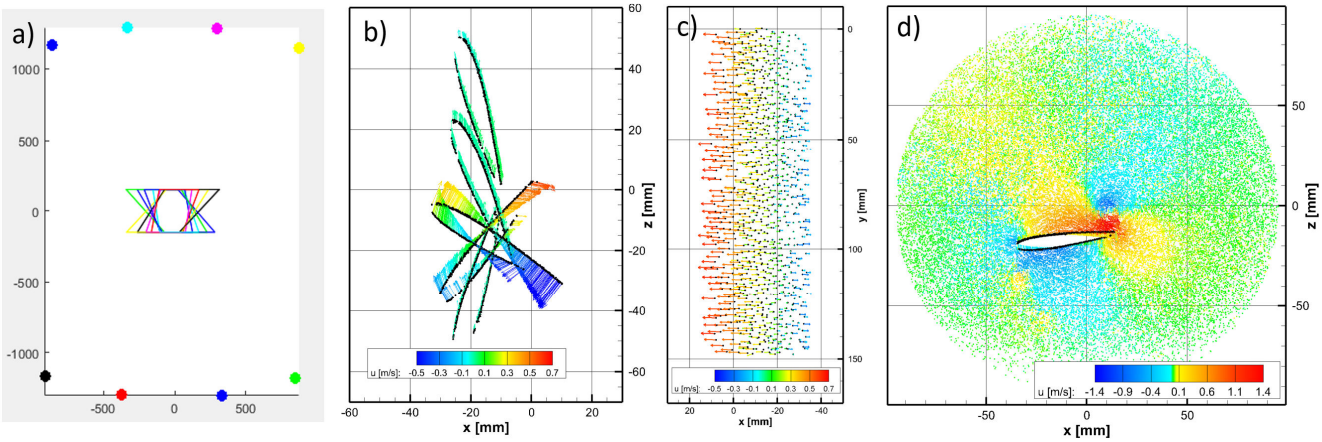

Figure 2: a) The calibrated camera setup, viewed from above. The camera lines-of-sight describe the commonly imaged volume; b) tracked wing markers with velocity vectors at four different phases of a combined ptiching and plunging movement, inspired by wing motion of hovering humming birds (viewed from above) ; c) side view of one phase of b); d) tracked particles at one time-step of the same hummin-bird-inspired movement, viewed from above. Tracked wing markers given as black dots.

Acknowledgements

This project has received funding from the European Union's Horizon 2020 research and innovation programme under grant agreement No 769237 HOMER.

References

Gesemann S, Huhn F, Schanz D, Schröder A, From noisy particle tracks to velocity, acceleration and pressure fields using B-splines and penalties. 18th Int. Symp. on Appl. of Laser and Imaging Tech. to Fluid Mech. Lisbon, Portugal, July 4 – 7, 2016

Huhn F, Getriebe für eine Auftriebsfläche, Schlagantrieb und Unterwasser- oder Luftfahrzeug, DE 10 2015 121 995, Deutsches Patent- und Markenamt, 2015

Jahn T, Schanz D, Schröder A, Advanced iterative particle reconstruction for Lagrangian particle tracking. Exp Fluids 62, 179, 2021.

Masateru M, Toshiyuki N, Ikuo K, Hiroto T, Hao L, Quantifying the dynamic wing morphing of hovering hummingbird. R. Soc. open sci. 4:170307, 2017

Schanz D, Gesemann S, Schröder A, Wieneke B, Novara M, Non-uniform optical transfer functions in particle imaging: calibration and application to tomographic reconstruction. Meas Sci Technol 24:024009, 2013

Schanz D, Gesemann S, Schröder A, Shake-The-Box: Lagrangian particle tracking at high particle image densities. Exp Fluids 57(5), 70, 2016

Schanz D, Novara M, Schröder A, Shake-The-Box particle tracking with variable time-steps in flows with high velocity range (VT-STB). 14th Int. Symp. on PIV (ISPIV 2021), Chicago, USA (online), 2021

Wieneke B, Volume self-calibration for 3D particle image velocimetry. Exp Fluids 45:549–556, 2007

Wieneke B, Iterative reconstruction of volumetric particle distribution. Meas Sci Technol 24:024008, 2013

Experimental study of buffet-induced fluid structure interaction on an OAT15A airfoil with a pitching degree of freedom

A. Accorinti[1*], *T. Baur* [1], *S. Scharnowski* [1], *C. J. Kähler* [1]
[1]Bundeswehr University Munich, Neubiberg, 85557, Germany

[*]alessandro.accorinti@unibw.de

Abstract

Shock buffet on airfoils occurs under certain combinations of transonic Mach number and angle of attack due to the interaction between the shock and the separated boundary layer. This flow instability leads to self-sustained shock oscillations, whose frequency is normally on the same order of magnitude as low structural Eigenfrequencies, which in turn can lead to fluid-structure interaction (FSI) and reduction in aircraft performance (Gao et al. 2020, Nitzsche et al. 2019). In order to improve the understanding of the FSI between buffet flows and airfoils, the flow over a supercritical profile (OAT15A) with a pitching degree of freedom is investigated at the Trisonic Wind Tunnel Munich by means of a combined application of Background Oriented Schlieren (BOS), Deformation and PIV measurements (see Figure 1). By applying these measurement techniques, all the involved contributions to the FSI can be observed, i.e. shock wave, structural response and boundary layer separation, respectively.

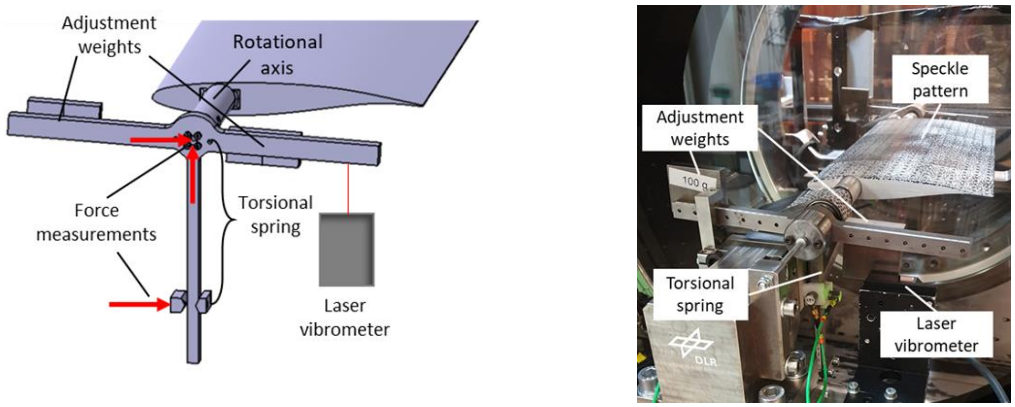

Figure 1: Experimental setup

BOS allows for a qualitative reconstruction of the density gradients in the flow by spatial cross-correlation with an undisturbed reference image. Figure 2a shows a raw image of the transonic flow with clear presence of a shock wave. In Figure 2b the resulting displacement obtained via cross-correlation is displayed. Furthermore, the results of an algorithm-based detection of the shock-position at different heights above the wing surface are visualized by means of black circles in the figure. Structural 3-D deformations of the wing are detected via stereo digital image correlation (DIC) measurements. In Figure 2c an example of the obtained deformation field with respect to wind-off conditions can be seen. The surface displacement can be decomposed into its components (see Figure 2d) and, in particular, the actual angle of attack can be computed, after subtraction of the torsional deformation with respect to wind-off condition. PIV measurements allow for the computation of the velocity field and the detection of the separated boundary layer region (see Figure 2e). By computing conditional averaged flow fields it is possible to analyze the development of the shock strength as well as the boundary layer separation during a buffet cycle (see Figure 2f). By comparing the power spectral density (PSD) of the shock location from BOS, of the streamwise velocity within the PIV fields and of the structural deformation, it is possible to investigate how buffet interacts with the structure (see Figure 2g-i).

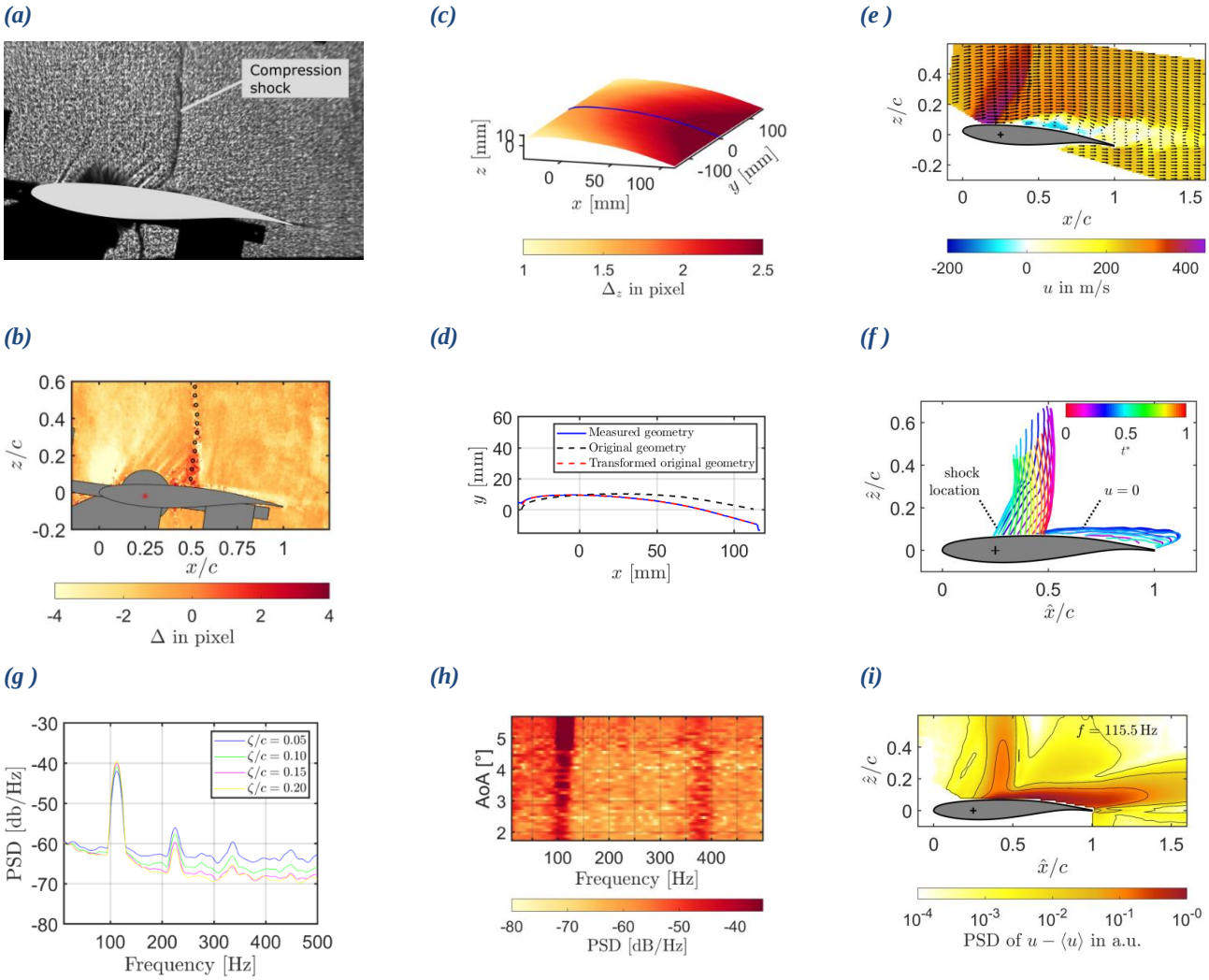

Figure 2: a) Raw image of BOS measurements exhibiting a shock on the airfoil suction side; b) Correlation-based surface tangential BOS displacement field; c) Surface displacement field; d) Measured surface contour; e) Instantaneous velocity field with separated boundary layer; f) Development of the shock and the separated region during a buffet cycle obtained via conditional averaging; g) PSD of the shock location fluctuations at several normal distances from the upper surface; h) PSD of the pitching motion of the airfoil for a sweep of the angle of attack; i) PSD of the velocity fluctuations at the buffet frequency

Acknowledgements

This project has received funding from the European Union's Horizon 2020 research and innovation programme under grant agreement No 769237 HOMER. Furthermore, the authors like to thank Jens Nitzsche, Yves Govers, Johannes Dillinger, Johannes Knebusch and Tobias Meier for their valuable contributions to the design of the experiment.

References

C. Gao, W. Zhang, 2020, "Transonic aeroelasticity: A new perspective from the fluid mode", Progress in Aerospace Sciences, Vol. 113, p.100596

J. Nitzsche, L. Ringel, C. Kaiser, H. Hennings, 2019, "Fluid-mode flutter in plane transonic flows", IFASD 2019 International Forum on Aeroelasticity and Structural Dynamics, 9-13 June, Savannah, Georgia, USA

Shock-Induced Panel Flutter Investigation with Simultaneous Use of PIV and DIC

A. D'Aguanno[1], P. Quesada Allerhand[1], ,F.F.J. Schrijer[1] and B.W. van Oudheusden[1]*
[1]*Aerodynamics Sect. (AWEP), Delft University of Technology, 2629 HS Delft, The Netherlands*

* a.daguanno@tudelft.nl

Abstract

The vibration of panel structural elements immersed in a supersonic flow is a fluid-structure interaction (FSI) that can affect the performance and structural integrity of supersonic aircraft and spacecraft systems. These adverse effects are further amplified when a shock-wave/boundary-layer interaction (SWBLI) is formed over the panel. This is of relevance, for example, in the operation of a non-adaptable nozzle (like that of a launch vehicle) in off-design conditions during the start-up. This results in an over-expanded flow that can lead to shock wave boundary layer interaction on the flexible nozzle wall, where impinging oblique shocks trigger violent oscillations of the nozzle (Pasquariello, 2018). A better understanding of this phenomenon, referred to as shock-induced panel flutter, is therefore crucial for the design of future high-speed vehicles.

In this study an experimental method is developed to study shock-induced panel flutter in the supersonic wind tunnel of TU Delft, the ST-15, a blowdown wind tunnel with a test section of 150 X 150 mm^2. The experiments have been carried out at a Mach number $Ma=2$, a total pressure $p_0=2.5\ bar$, and a total temperature $T_0=288\ K$. The test panels are made in AL7075-T6 with a thickness of 0.3 mm and incorporated in the bottom liner of the wind tunnel test section by the use of two clamping pieces. The panels have been clamped only at the leading edge and at the trailing edge (clamped-clamped-free-free conditions, CCFF) and have an aspect ratio $a/b=1.5$ (indicating with $a=126\ mm$ the length of the panel and with $b=84\ mm$ the width). An additional rigid panel has been used as reference. The presence of an impinging shockwave on the panel has been ensured by the use of an 11° shock generator. An overview of the different elements present in the wind tunnel test section is shown in Figure 1-left. Shock induced panel flutter strongly depends on the specific clamping conditions, nevertheless, only limited studies are present in literature on CCFF panels. Therefore, the reported findings could serve as a reference for future researchers when designing both experimental and numerical simulations of shock induced panel flutter, particularly if two-dimensional flutter is to be recreated.

For this research, two optical techniques have been used: planar particle image velocimetry (PIV) and stereographic digital image correlation (DIC). The measurements have been carried out simultaneously to obtain the full-field structural displacement of the panel and the corresponding flow field around it (with the PIV measurement plane passing in the mid span of the panel). In order to avoid interference between the PIV and DIC systems, an optical isolation system has been devised using fluorescent paint, dedicated light sources, and colour lens filters. The use of these techniques for similar applications has already been recorded in literature by Spottswood et al. (2019), however, to the best of the authors' knowledge there is no study in which they have been used simultaneously for studying shock-induced panel flutter. An image of the speckle pattern illuminated by blue LEDs is shown in Figure 1-right.

The acquisition frequency of the cameras (5 kHz) has allowed to time resolve the oscillation of the panels and of the reflected shockwave. A following spectral analysis has shown a frequency of oscillation of 420 Hz for both the thin panel and the reflected shockwave. In addition, for the PIV data, a low-frequency dynamics of the SWBLI during the interaction is observed. In Figure 2, the simultaneous PIV and DIC fields are shown for four images taken from a complete flutter cycle on the CCFF panel (with a time spacing of $\Delta t=0.6$ ms). The PIV images show the presence of the impinging shockwave (SW), separated area and oscillating reflected SW. The latter is located in its most upstream position in the first snapshot (image on the top left) and in its most downstream position in the third snapshot (for $t=t_0+1.2$ ms). The DIC images confirmed the presence of a phase delay between the panel displacement and the reflected SW position, with the most upward panel displacement being observed in the second snapshot (image on the top right) and the most downward in the last snapshot.

The knowledge of the reflected shock position and of the panel displacement has allowed the computation of a phase average for both the panel displacement and the flow field, extracting the average behaviour in the different flutter

phases. Finally, the coupling of the displacement of the panel and the SWBLI has also been studied, identifying the regions of maximum correlation in the flow between the panel motion and the flow velocity fluctuations. The obtained results suggest that the inviscid flow region upstream of the SWBLI (located between the leading edge of the panel and the reflected SW position) may play a significant role in the fluid-structure interaction.

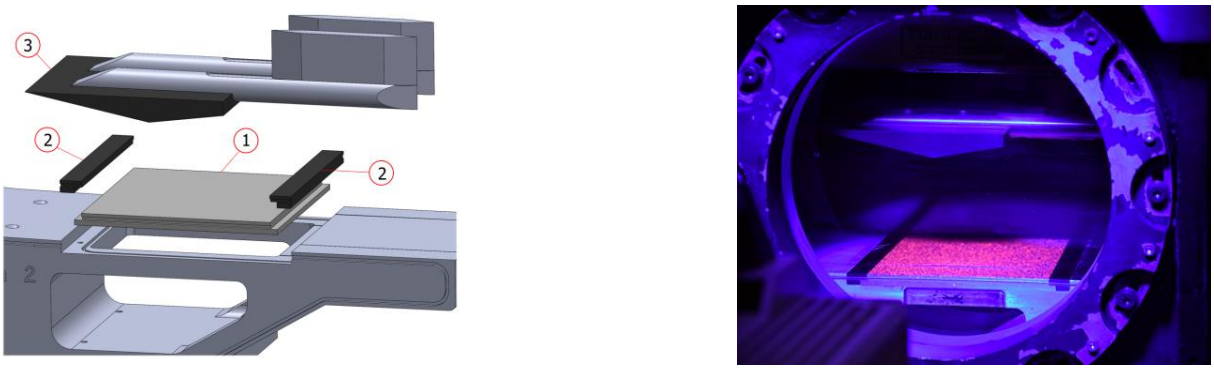

Figure 2: CAD model of the wind tunnel test section, with panel (1), clamping pieces (2) and shock generator (3) (left). Speckle pattern of the CCFF panel illuminated by blue LEDs (right).

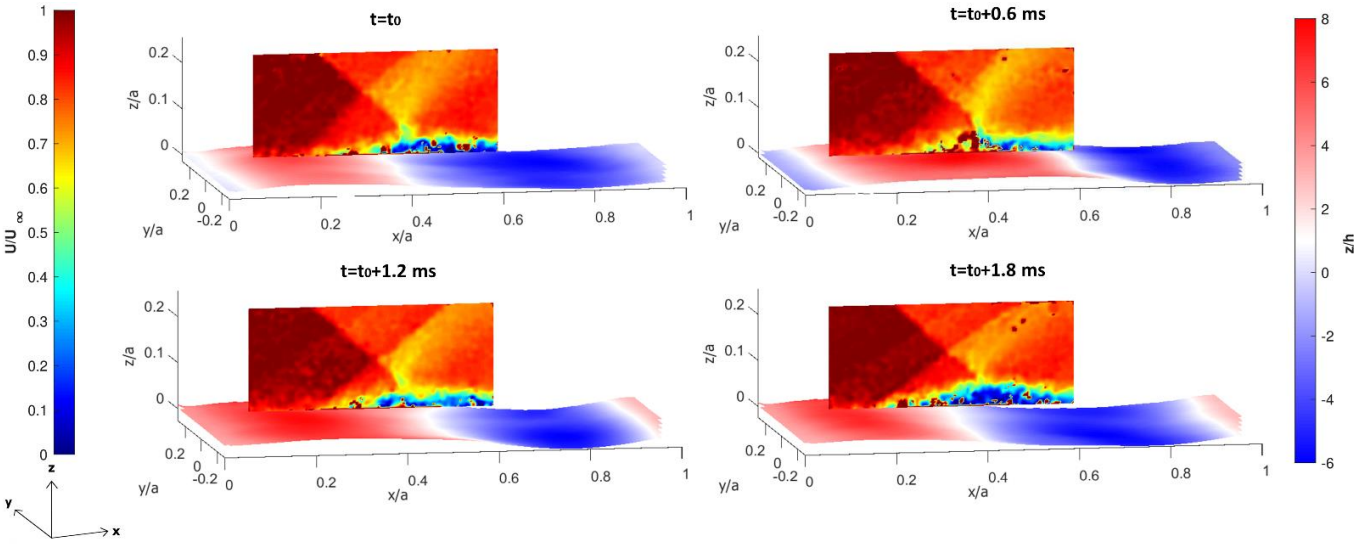

Figure 2: Simultaneous flow (PIV) and structure (DIC) fields for four time steps (with a spacing of Δt=0.6 ms) taken from a complete flutter cycle

Acknowledgements

This project has received funding from the European Union's Horizon 2020 research and innovation programme under grant agreement No 769237 HOMER.

References

Pasquariello, V., Analysis and Control of Shock-Wave/ Turbulent Boundary-Layer Interactions on Rigid and Flexible Walls. *PhD thesis*, Technische Unversität München, 2018.

Spottswood, S. M., Beberniss, T. J., Eason, T. G., Perez, R. A., Donbar, J. M., Ehrhardt, D. A., Riley, Z. B., Exploring the response of a thin, flexible panel to shock-turbulent boundary-layer interactions, Journal of Sound and Vibration, 443, pp. 74-89, 2019.

Experimental study of fluid-structure interactions on Darrieus turbines

L. Kara Mostefa L. Chatellier L. Thomas
Institut PPRIME, UPR3346, CNRS – Université de Poitiers – ISAE-ENSMA, France

Mohamed.larbi.kara.mostefa@univ-poitiers.fr

Abstract

Both scientific and industrial communities have a growing interest for marine renewable energies. There is a wide variety of technologies in this domain, with different degrees of maturity. Our work focuses on two models of a H-type vertical axis Darrieus (1931) tidal turbine with the objective of studying the effect of fluid-structure interactions on their performances. The first prototype comprised four straight rigid blades maintained by circular flanges on both ends of the rotor (Figure 1a), and is a down-scaled model of the one used in the study of Gorle et. al (2016). The second model is equipped with free-ended interchangeable blades attached to a single flange (Figure 1b). A configuration of the second model mounted with rigid stainless steel blades is first used for comparison with the dual-flange turbine, then a configuration using PEEK blades of significantly lower Young modulus is investigated in order to address the fluid-structure interaction problem. Both turbine models have a rotor diameter of 400mm and 80mm-chord NACA0015 blades of 400m length.

The experimental studies are carried out in the 15m long and 1m² square section free surface channel of the Environmental Hydrodynamics Platform at PPRIME Institute (Figure 1c). The maximum flow discharge through the channel is Q = 500 l/s, leading to maximum respective chord- and diameter-based Reynolds numbers of 2×10^5 and 3.5×10^5, depending on the water level and tip-speed ratio.

(a) (b) (c)

Figure 1 : Dual- (a) and single-flange (b) straight blade H-type Darrieus turbines ; free surface hydrodynamic channel (c).

The rotor is driven by a servo motor and equipped with torque and angular position sensors. Torque measurements are first carried out to characterize the performances of the turbines in a range of operating conditions with different combinations of water level, flow discharge and tip-speed ratios. For optimal regimes of the two turbines, PIV and blade deformation stereoscopic measurements are carried out in phase-locked conditions.
The PIV measurements are conducted within the mid-plane of the rotor using two double-cavity 532nm ND:YAG laser and one LaVision Imager LX 16M CCD camera. The camera is positioned below the glass bed of the channel and image the measurement zone through a 45° mirrors, covering 3 rotor diameters stream-wise and 2 rotor diameter cross-wise. The combination of the 16MP and two angled laser sheets thus allows to limit the masking of the measurement zone during the passage of the blades (Figure 2a) while providing an enlarged field of view. The PIV timing sequence is adjusted so that successive velocity fields correspond to an angular displacement multiple of 7.5°, ensuring a well resolved coverage of the rotational cycle of the turbine.

The stereoscopic measurements are conducted using two LaVision Imager Pro X 4MP CCD cameras in vertical stereoscopic arrangement on the side of the flume (Figure 2b). The lighting device consists of different combinations of a 200W Floodlight LED panel, HARDSoft IL-106X 528nm pulsed diodes, and Veritas Constellation 120E LEDs, arranged to provide illumination of the moving blades over their full path. In order to allow measurements of the blades positions and deformations during the turbine rotation cycle, the individual blades are respectively painted with random speckle patterns or cartesian dot grids. The corresponding images pairs are processed using triangulation of the apparent grid dots. (Figure 2).

(a) (b)

Figure 2: Overview of the PIV (a) and stereoscopic (b) measurement setups.

The combination of PIV measurement (Figure 3a) and blade surface reconstructions (Figure 3b) allows to link the blade deformation with the flow features and rotor kinematics leading to the highly fluctuating torque. Of particular interest are the interactions between the blade and the vortex shed due to dynamical stall in the upstream part of the rotation cycle. For tip-speed ratios in the range of the optimum values of λ=2.15-2.3, the shed vortex is advected towards the downstream part of the rotor before being reached by the incoming blades moving at higher azimutal velocity. The interaction between the blades and shed vortices results in fluctuating loads which are investigated by associating flow diagnostics, and blade deformation measurements.

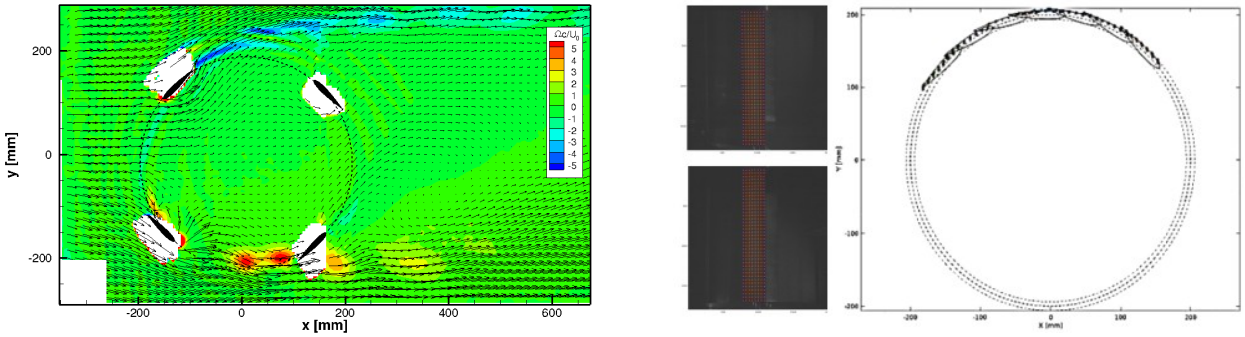

(a) (b)

Figure 3: Sample examples of PIV at the optimum TSR (a) and stereoscopic reconstruction (b) results.

Acknowledgements

This work and ML Kara-Mostefa's PhD were funded by the ANR project DYNEOL (ANR-17-CE06-0020)

References

Darrieus G, Turbine having its rotating shaft transverse to the flow of the current, 1,835,018, 8 December 1931
Gorle JMR, Chatellier L, Pons F, Ba M, Flow and performance analysis of H-Darrieus hydroturbine in a confined flow: A computational and experimental study. Journal of Fluids and Structures 2016; 66 :382–402, 2016

Data Assimilation

Towards the closure of Collar's triangle by optical diagnostics

G. Gonzalez Saiz[1*], *A. Sciacchitano*[1], *F. Scarano*[1]
[1]Faculty of Aerospace Engineering, Delft University of Technology, Delft, The Netherlands
[*]g.gonzalezsaiz@tudelft.nl

Abstract

Weight reduction in flying systems has been the focus of the past decades as a strategy to increase the sustainability of aviation. However, light-weight structures are increasingly prone to large deformations and non-linear aeroelastic phenomena, whose computational modelling is recognized as a challenge. In this context, aeroelastic experiments are hindered by the complexity of the setups. The latter usually require either models instrumented with sensors, or the use of several optical systems synchronized to conduct non-intrusive simultaneous measurements of flow fields and structural deformations. The current work proposes an experimental methodology that locally evaluates the three key contributors to Collar's triangle of forces, namely aerodynamic, elastic, and inertial forces.

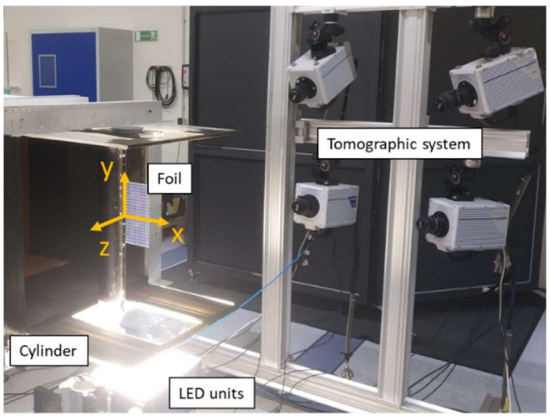

Figure 1: Experimental setup

The methodology is applied to a benchmark problem of fluid-structure interaction, featuring a flexible transparent foil attached to the trailing edge of a circular cylinder at low-speed conditions (free-stream velocity of $U_\infty = 2.25\ m/s$, $Re = 13{,}500$ based on the cylinder's diameter). The foil is speckled with a pattern of bright markers and the flow is seeded with Helium Filled Soap Bubbles (HFSB, Scarano et al. 2015). The position of flow tracers as well as of markers on the object surface is monitored by a volumetric Particle Tracking Velocimetry (PTV) system based on four high speed cameras. The images are analyzed with Lagrangian particle tracking techniques and the flow tracers and surface markers are separated based on the different properties of their images within the tracking algorithm (Shake-The-Box, STB, Schanz et al. 2016).

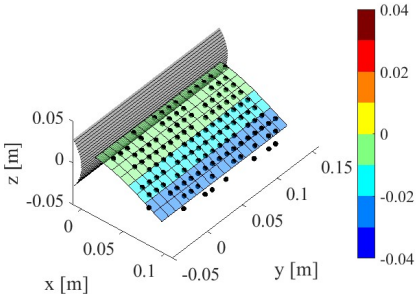

Figure 2: Structural description of the foil, including tracked markers in black dots and a contour of displacement on the reconstructed surface.

The inertial and elastic forces are obtained solely by analyzing the motion and the deformation of the foil. A fifth order surface is fitted through the tracked surface markers over a time stencil of 1/10 of a cycle to regularize the data and reduce the measurement noise. The inertia force is calculated from the acceleration of the foil, i.e. second time derivative of the displacement, and the mass of the foil. According to the Kirchhoff-Love theory for plates under pure bending, elastic forces are calculated from the fourth spatial derivative of the deformation. For the aerodynamics, flow velocity fields are obtained by fine gridding the tracked flow tracers by means of VIC# (Jeon et al. 2018). The pressure loads on the panel are then evaluated by solving the Poisson equation for pressure within the flow field (van Oudheusden, 2013).

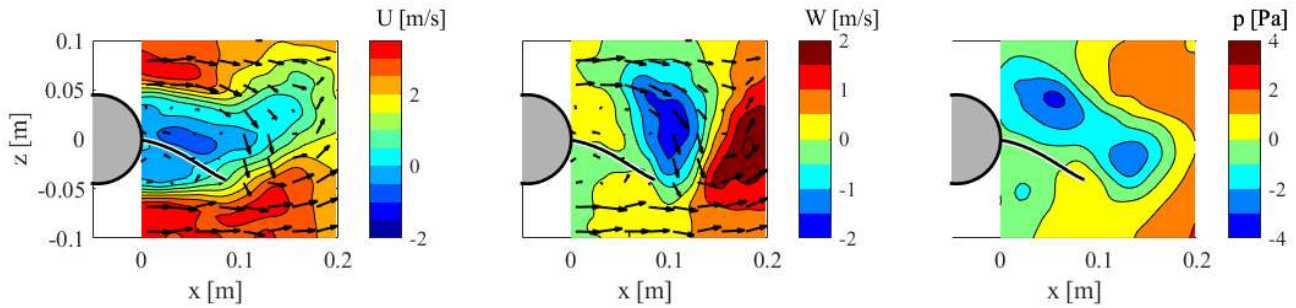

Figure 3: Countours of velocity fields: streamwise (left) and transverse (center), and pressure field (right).

A view of the reconstructed foil surface at a reference time (down-most position) with a contour of the displacement and the tracked markers is given in Figure 2. The grided velocity fields (streamwise and transverse) and the computed pressure field at the latter time are shown in Figure 3.

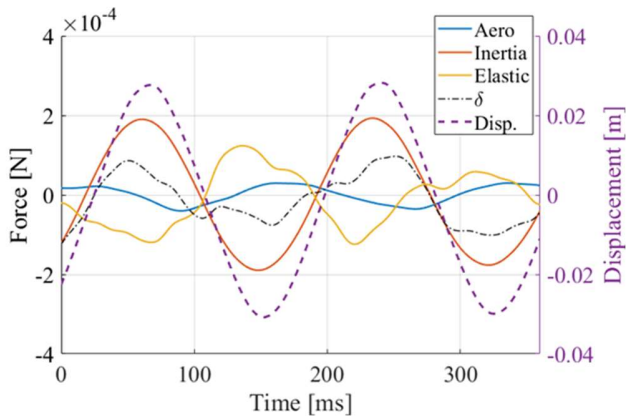

Figure 4: Instantaneous time-evolution of aeroelastic forces: aerodynamic (blue), inertial (red), and elastic (yellow) for the location (mid-height and 0.75 chord). The sum of forces is drawn in black dash-dotted. Z-position (purple dashed) is given as reference (right y-axis).

The time-evolution of the computed aeroelastic forces is extracted at a particular tile location (mid-height and 0.75 chord) and presented in Figure 4. The trends of the loads are consistent with the underlying physical mechanisms. The inertia force is in phase with the foil's displacement, as it opposes the acceleration of the foil. The elastic loads react to the deformation of the body bringing it to the non-deformed state, and so they exhibit the opposite trend with respect to the displacement. Finally, aerodynamics is the forcing agent (external force) of the system. The motion of the foil shows a delay of roughly $\varphi \approx \pi/4$ with respect to the aerodynamic force due to the structural damping. In addition, the overall aerodynamic force level is lower than the inertia and the elastic loads, mainly because a low amount of energy is needed to maintain the periodic motion of the foil once the latter is oscillating.

The closure of Collar's triangle, i.e. the equilibrium of Collar forces, is evaluated locally (Figure 4) by means of the residual $\delta = F_{aero} + F_{elastic} + F_{inertia}$. The latter reaches 30% of the reference force (maximun inertia). The reason for a non-null residual is ascribed to the uncertainty of the elastic loads, being the latter proportional to the fourth spatial derivative of the foil's displacement.

To conclude, a non-intrusive measurement methodology for aeroelastic experiments based on the Lagrangian particle tracking technique is proposed to simultaneously estimate aerodynamic, elastic, and inertial loads from a deforming model. Such methodology offers a wide spectrum of information (flow fields, flow topology, fluid loads, structural deformations, in-plane strains, and structural loads) for a compact system, characteristic of 3D PIV measurements (4 camera tomographic system). Moreover, the simultaneous estimation of the main forces involved in an aeroelastic experiment implies the ability to close Collar's triangle of forces.

Acknowledgements

This project has received funding from the European Union's Horizon 2020 research and innovation programme under grant agreement No 769237 HOMER.

References

Jeon YJ, Schneiders JF, Müller M, Michaelis D, Wieneke B. 4D flow field reconstruction from particle tracks by VIC+ with additional constraints and multigrid approximation. In Proceedings 18th International Symposium on Flow Visualization 2018 Oct 5. ETH Zurich.

Van Oudheusden BW. PIV-based pressure measurement. Measurement Science and Technology. 2013 24;24(3):032001.

Scarano F, Ghaemi S, Caridi GC, Bosbach J, Dierksheide U, Sciacchitano A. On the use of helium-filled soap bubbles for large-scale tomographic PIV in wind tunnel experiments. Experiments in Fluids 2015; 56(2):1-2.

Schanz D, Gesemann S, Schröder A. Shake-The-Box: Lagrangian particle tracking at high particle image densities. Experiments in fluids. 2016; 57(5):1-27.

Dynamic mode decomposition-based reconstructions for fluid-structure interactions: An application to membrane wings

E. Rodríguez-López [1], *D. W. Carter*[1], *B. Ganapathisubramani*[1*]

[1]University of Southampton, Southampton, UK
*:g.bharath@soton.ac.uk

Abstract

Four data-driven low-order modelling approaches, Dynamic mode decomposition (DMD) and three other variations (optimal mode decomposition, total-least-squares DMD and high-order DMD), are used to capture the spatio-temporal evolution of fluid-structure interactions. These methods are applied to experimental data obtained in a flow over a flexible membrane wing and its elastic deformation. Spectral coherence indicates there exists an interaction between the flow and structural deformation at a single frequency for this problem (depending on the angle of attack and/or the presence of a ground). It is therefore an ideal data set to assess the performance of the four different methods in terms of the relevant modes/frequencies and reconstruction of flow and structural deformation. We show that the four methods detect the same dominant frequency (within Fourier resolution) and qualitatively the same associated mode. However, the modes appear to be heavily damped or amplified preventing a successful flow and structure reconstruction (except when using high-order DMD). This problem persists even if the damping coefficients are set to 0 due to imprecision in the estimation of the dominant frequency. The reconstruction is assessed by means of the average correlation between the real and reconstructed fields corresponding to 0.42 and 0.85 for the fluid and membrane deformation respectively when using high-order DMD (and virtually 0 for the other three methods). Based on the analysis, we conclude that high-order DMD, particularly for when fluid and structural data are modelled simultaneously, is the most suitable method to generate linear low-order models for fluid-structure interaction problems. Further, we show that this modelling is not dependent on the relative energies of fluid and membrane deformation.

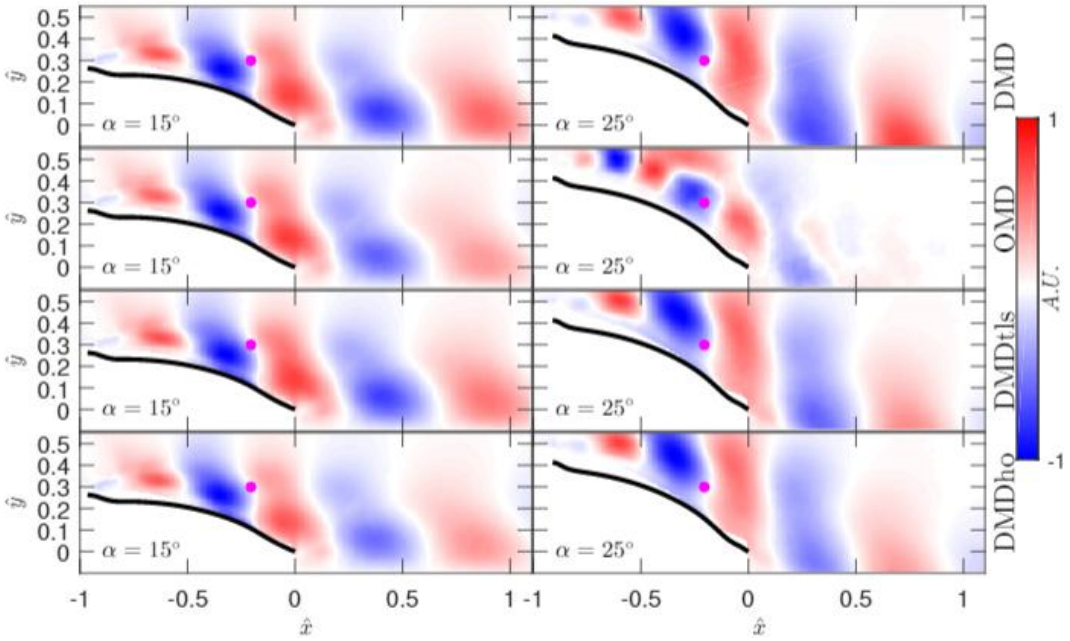

Figure 1: Real part of the characteristic flow mode $\phi_\star^v$ (at frequency $St^\star$) for various decompositions and the two angles of attack. The modes are arbitrarily normalized such that the imaginary part of $\phi_\star^v$ at the location of the pink dot ($\hat{x} = -0.2,\ \hat{y} = 0.3$) is null.

Acknowledgements

This project has received funding from the European Union's Horizon 2020 research and innovation programme under grant agreement No 769237 HOMER.

Data assimilation method for RANS using time-averaged PIV of the flow around a two-dimensional airfoil

C.Thompson[*], *S.Symon, B.Ganapathisubramani*

[*]ct4g16@soton.ac.uk

Abstract

CFD using a RANS approach is a time efficient method to simulate aerodynamic problems, however from previous investigations RANS simulations have difficulty predicting the transition, separation and reattachment locations on the suction side of stalled airfoils.

With the introduction of PIV, velocity flow fields around airfoils can be obtained experimentally and used to drive CFD simulations, thereby computing more accurate predictions. The resultant predictions can be used to generate missing flow fields, tune simulation parameters, or investigate the far field away from the measurement domain.

Data assimilation was first conducted on two-dimensional RANS mean flows by Foures et al. [1] showing the value of using data assimilation to recover more information about the flow than is directly measurable. More recent work by Saredi et al. [2] shows how data assimilation can be used to improve three-dimensional RANS simulations. The separation and recirculation region behind a bluff body were more accurately predicted when using a spatially varying forcing term within the momentum equation. Work by Mons and Marquet [3] show how data assimilation can be used to determine optimal probe placement strategies, aiming to reconstruct mean flow from two-dimensional RANS simulations.

In this investigation a state observer-based data assimilation approach is used to improve a steady two-dimensional incompressible RANS simulation of a NACA0012 airfoil in pre, transition and post stall conditions. The investigation shows how an additional spatially constant forcing term within the RANS equation can be optimized to generate a more accurate prediction of the flow field, the physical understanding and significance of this forcing term is explored. For the transitional case, optimal probe placement methods including POD reconstruction, nominal spacing and measurement uncertainty are used to determine the locations of interrogation positions, the results of which are evaluated for accuracy and time efficiency.

Experimental stereoscopic PIV was carried out on a rigid wing, a NACA0012 airfoil was placed within a water flume in the University of Southampton. The airfoil had a chord of 0.15m and was subjected to a Reynolds number of 7.5×10^4 at angles of 4, 13 & 15 degrees. The experimental domain was 230 mm in the streamwise direction and 190 mm in the vertical direction with a 270 x 220 uniform grid of measurement points. 5467 images were acquired for each angle of attack at a rate of 1000 Hz.

OpenFoam is an open source CFD solver used in this investigation [4]. The functions and equations within openFOAM are modified to include the necessary forcing term for data assimilation. The incompressible SIMPLE algorithm is used as the solver for the continuity and momentum equation. A RANS approach with a two-equation linear eddy viscosity $k-\omega$ shear stress transport model is used; this model is computationally cheap and can capture flow separation [5]. The simulation has four degrees of freedom, the solution for $U, p, k \,\&\, \omega$ (velocity, pressure, turbulent kinetic energy and turbulent dissipation rate) are computed at each grid location. The mesh used is a well-documented and validated 225 x 65 NASA C-grid (where the chord length is 1), developed at the Langley Research Center. The mesh is displayed in (Figure 1) and can be found here [6]. The grid has 14,336 internal query positions and 128 points on the airfoil surface, in contrast to the 59,400 experimental points.

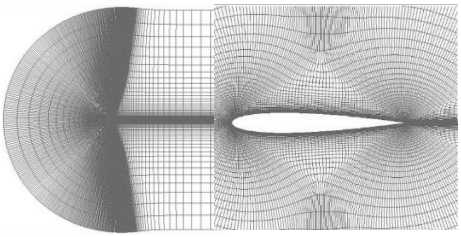

Figure 1: (Left) The total 225 x 65 NASA C-grid, (right) a zoomed in view of the mesh surrounding the airfoil.

To determine improvements to the simulation following data assimilation, first a baseline simulation is computed. Initially all the experimental data positions are used as interrogation locations by interpolating the CFD results. An average of the L1 error is calculated using Eq(1.), which is also used as the objective function when optimizing the forcing term, shown in Eq(2.). The magnitude of the forcing term is determined using the Nelder-Mead simplex algorithm [7], chosen due to its robust nature.

$$Error_{L1} = mean\left(\left|U_i^{experiment} - U_i^{simulation}\right| + \left|V_i^{experiment} - V_i^{simulation}\right|\right)/U_{inf}, \quad (1.)$$

$$U_j^* \frac{\partial U_i^*}{\partial x_j^*} = -\frac{\partial P^*}{dx_i^*} + \frac{1}{Re}\frac{\partial^2 U_i^*}{\partial x_j^* \partial x_j^*} - \frac{\overline{\partial u^{*\prime}_i u^{*\prime}_j}}{\partial x_j^*} + f_i, \text{where } f_i = [a_1, a_2] = const. \quad (2.)$$

When using the full experimental domain as interrogation positions, improvements of 43%, 62% & 34% within 20, 30 & 40 iterations for angles of 4, 13 & 15 degrees respectively were observed compared to the baseline simulation. For the 13 and 15 degree cases, the improvements are visible within the shear layer between the free stream and recirculation region, shown in (Figure 2). The forcing term can be evaluated as an additional lift and drag component, which are observed to be constant with 0.000149% additional lift and 0.000127% additional drag.

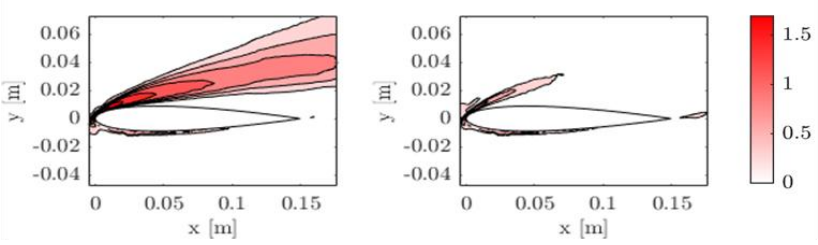

Figure 2: A contour plot of the L_1 error between the, (Left) baseline simulation, (Right) data assimilation, and experimental data.

When reducing the number of interrogation locations within the domain uniformly, a reduction in computational time and increase in error was observed compared to using all positions. When using a POD based reconstruction to determine 100 interrogation locations, there was an increase in error compared to the baseline simulation. When using experimental uncertainty to determine 100 interrogation locations, it was found a further error reduction of 10% was observed compared to using all interrogation locations, as well as a decrease in computational time.

Acknowledgements

Experimental data acquired from Dr. Douglas Carter is acknowledged in providing a basis for this investigation.

Financial support from EU grant HOMER is gratefully acknowledged.

References

[1] D. P. G. Foures, N. Dovetta, D. Sipp, and P. J. Schmid, "A data-assimilation method for Reynolds-averaged Navier–Stokes-driven mean flow reconstruction," *J. Fluid Mech.*, vol. 759, pp. 404–431, Nov. 2014, doi: 10.1017/jfm.2014.566.

[2] E. Saredi, N. Tumuluru Ramesh, A. Sciacchitano, and F. Scarano, "State observer data assimilation for RANS with time-averaged 3D-PIV data," *Comput. Fluids*, vol. 218, p. 104827, Mar. 2021, doi: 10.1016/j.compfluid.2020.104827.

[3] V. Mons and O. Marquet, "Linear and nonlinear sensor placement strategies for mean-flow reconstruction via data assimilation," *J. Fluid Mech.*, vol. 923, p. A1, Sep. 2021, doi: 10.1017/jfm.2021.488.

[4] "OpenFOAM | Free CFD Software | The OpenFOAM Foundation." https://openfoam.org/ (accessed Jun. 17, 2021).

[5] F. R. Menter, "Two-equation eddy-viscosity turbulence models for engineering applications," *AIAA J.*, vol. 32, no. 8, pp. 1598–1605, Aug. 1994, doi: 10.2514/3.12149.

[6] "Grids - NACA 0012 Airfoil." https://turbmodels.larc.nasa.gov/naca0012_grids.html (accessed Jun. 17, 2021).

[7] J. A. Nelder and R. Mead, "A Simplex Method for Function Minimization," *Comput. J.*, vol. 7, no. 4, pp. 308–313, Jan. 1965, doi: 10.1093/comjnl/7.4.308.

Aeroelasticity

An experimental investigation on stall flutter over a vertically mounted rigid finite wing

R. F. Soares[1*], I.Karasu[2], B. Ganapathisubramani[1]

[1] University of Southampton, Southampton, SO17 1BJ, United Kingdom

[2] Adana Alparslan Turkes Science and Technology University, 01250, Saricam, Turkey

* R.F.Soares@soton.ac.uk

Abstract

As stall flutter has relevant engineering implications, such as in blades of wind turbine and HALE (high-altitude long-endurance aircraft). This work presents the experimental investigation of rigid wing setup in a closed-circuit wind tunnel having 2.1 *m* × 1.5 *m* test section. The experimental campaign reached stable and symmetrical LCO within the freestream range from 9 *m/s* up to 14 *m/s* ($1.69 \times 10^5 < Re < 2.63 \times 10^5$). Two techniques were used for position tracking: one mechatronic and one image-based. The latter used 'shake-the-box' method applied to a body, which has proven a successful approach as a non-intrusive tool.

1 Introduction

The experiments were carried out at the 7x5 Wind Tunnel; a closed-circuit facility with two test sections in serial. For this experiment, the setup was installed at the high-speed test section (2.1 *m* × 1.5 *m*). The wing is a NACA0012 cross-section model of aluminium (.e. structure) and carbon-fibre composite (e.g. skin) of 0.3*m* chordwise and a span length of 0.77 *m*. A servo motor with cylindrical shield is the base for the wing, which was connected to a 6-axis Delta IP65 load cell.

In the heaving axis, the system was attached to a pair of linear-guided carriages, and the nominal rest position is found after two identical, counterbalance springs were linked, providing a spring constant (k) of 400 *N/m*. In the pitching axis, one pair of identical rubber bands were used on each side, connecting the wing leading edge to the cylindrical base.

The image-based tracking solution involved Particle Tracking Velocimetry (PTV) with 'shake-the-box' methodology, where 5 Phantom V641 high-speed cameras recorded a scattered pattern of 8mm dots on the wing surface. Experimental setup is illustrated in Figure 1.

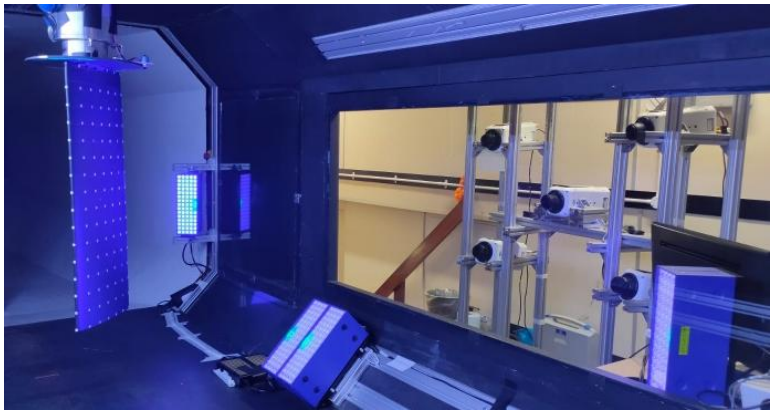

Figure 1: Wing system and 'shake-the-box' hardware setup for structural analysis.

2 Summary of Results

Both position tracking tools were performed simultaneously and lately compared in order to assess the quality of the image-based technique as a surface tracking tool. The later were processed in two steps: (i) obtaining the time-resolved position tracking with 'shake-the-box' methodology, then (ii) reconstruction of the wing surface and estimation of the angular and heaving history. Assuming the mechatronic position tracking results as baseline, the non-intrusive results are compared and presented in Figure 2.
A nominally harmonic dataset were found for each self-sustained LCO, which allowed analysis in phase-averaged format (Figure 3), where the properties are averaged as a function of the angle of attack cycle (i.e. pitching motion) discretised within 1° resolution.

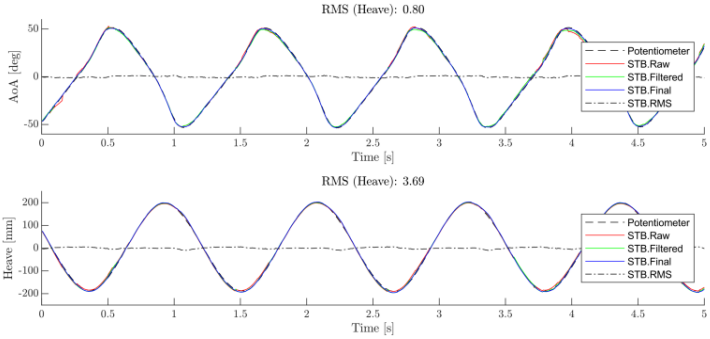

Figure 2: Position tracking validation: mechatronic- vs image-based systems.

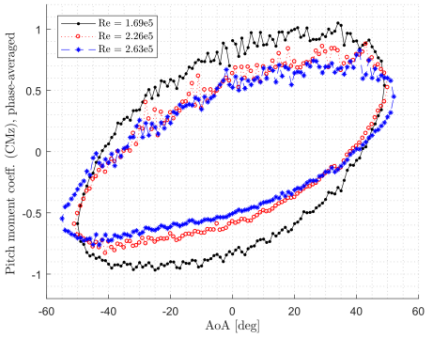

Figure 3: Phase-averaged LCO's.

3 Conclusions

The occurrence of a self-sustained LCO were found of the system with a NACA0012 rigid wing. An initial perturbation was required to trigger the phenomenon; however, the motion amplitudes were noticeably stable and reproducible for a same trigger input.The absolute minimum freestream able to sustain the motion was 8.5m/s with minor decay instabilities, and any freestream higher than 14 m/s would reach the physical end-stops. The 'Shake-the-Box' method applied as a body tracking solution has been successfully validated, allowing the use of this approach as a non-intrusive tool for further applications.

Acknowledgements

We gratefully acknowledge the financial support from EU H2020 project HOMER (Grant Ref No: 769237).

References

[1] G. Dimitriadis and J. Li, "Bifurcation Behavior of Airfoil Undergoing Stall Flutter Oscillations in Low-Speed Wind Tunnel," AIAA Journal, vol. 47, no. 11, pp. 2577–2596, Nov. 2009.

[2] D. Poirel and F. Mendes, “Experimental Small-Amplitude Self-Sustained Pitch–Heave Oscillations at Transitional Reynolds Numbers,” AIAA Journal, vol. 52, no. 8, pp. 1581–1590, Aug. 2014.

Workshop on Optical Metrology and Data Assimilation Applied to Aeroelastics
Sept. 22-23, 2021 | TU Delft, NL & Online

Pitsching wing in Fluid-Structure Interactions

G. Acher[1], P.Braud[1], L. Chatellier[1], L. Thomas[1], L. David[1]
[1]Institut PPrime, UPR 3346, CNRS-Université de Poitiers-ENSMA, France
[*] Laurent.david@univ-poitiers.fr

Abstract

In high incidence conditions, wings are subjected to large vortex detachments which promote the dynamic stall leading to a sudden drop in lift. Under such conditions it is often necessary to modify the lifting surface so that the effective angle of attack is reduced, or prevent vortex shedding by using actuators such as plasma actuators or micro jets with the objective of moving the point of detachment away from the leading edge. Another way to reduce these massive detachments is to force pitching of the profile with a low amplitude around the characteristic frequencies of this vortex shedding. The object of the study is therefore to study the modifications of the flow in a case of a pitching wing around a position of high incidence and to measure the effects of this oscillation on the near wake , and simultaneously to look at the mechanical effects produced on the wing.

In this paper, measurements of the 3D deformation of a NACA0015 flexible wing profile installed at a large angle of attack and pitching with small amplitude around the natural vortex shedding frequency at a Reynold number of 10^5 are applied simultaneously with 3D flow measurements. Wing time-deformation, volumetric instantaneous velocity fields are measured and correlated to show mutual influence between the flow and the wing.

Setups and apparatus

A wing profile of 146 mm span is placed at 15° angle of attack in the test section of a hydrodynamic tunnel. The NACA0015-type wing profile, based on a 80 mm chord, is built of a 140 mm long straight section and its tip is formed by the rotation of the profile around the chord, adding 6mm of wingspan, at the position of maximum thickness. The profile is oscillating with an amplitude of 2 and 4° around the initial angle of incidence at different frequencies around the natural frequency of the vortex shedding (f=5 and 9.4 Hz). The surface of the wing is monitored by two high speed cameras so that both the pitching motion and deformations are characterized. Four other high speed cameras are used to investigate the instanteous flow fields using Lagrangian Particle Tracking.

Results

Time resolved estimation of the wing motion and deformation is obtained using the PIV/DIC method described by Chatellier et al. (2013). The technique is based on maximizing the correspondence of two back-projected images on the estimated solid surface. In order to follow the deformation of the wing profile in the test section, a speckle pattern is painted on its pressure side so that the two high speed cameras placed under the water tunnel image the full wingspan. An example of results is presented in Figure 1.

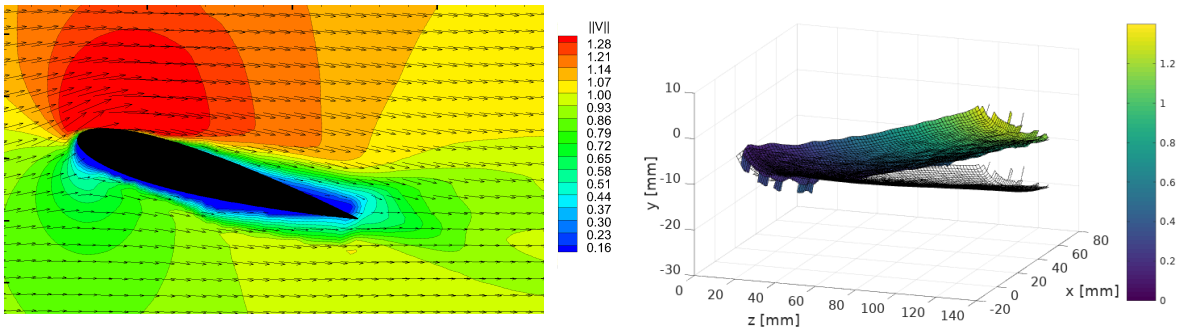

Figure 1: Sample LPT and DIC result.

The flow velocity field is measured using Shake-The-Box algorithm (Schanz et al, 2016) in order to provide 3D time-resolved particle tracks from the four camera recordings. Velocity and acceleration are extracted (figure 2) and allow to calculate the main characteristics of the flow in terms of vorticity, Q criteriin and pressure-from-PIV estimates (Jeon et. al, 2016).

Correlation between the solid and fluid databases are then calculated to estimate the interaction between the fluid and structure and allow to understand the effect of the flexible wing for wake minimization and drag reduction.

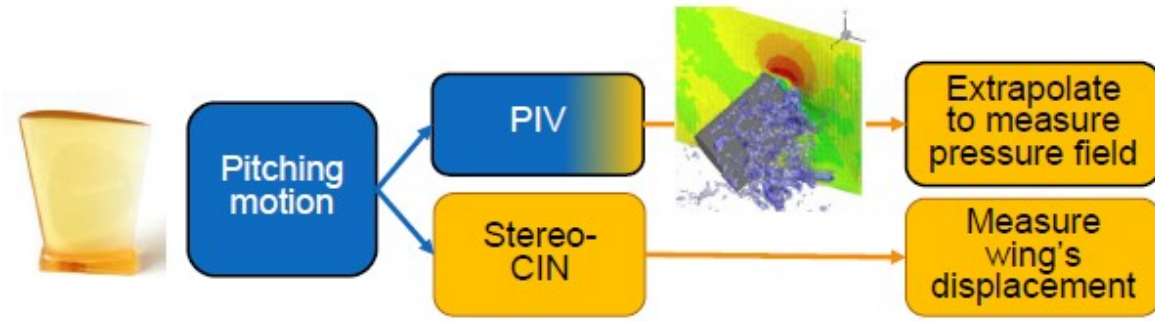

Figure 2: Experimental and numerical FSI framework.

Acknowledgements

This project has received funding from the European Union's Horizon 2020 research and innovation programme under grant agreement No 769237 HOMER.

References

Chatellier L, Jarny S, Gibouin F, David, L (2013) A parametric PIV/DIC method for the measurement of free surface flows. Experiments in fluids, 54(3), 1488.

Schanz D, Gesemann S, and Schröder A (2016) Shake-The-Box: Lagrangian particle tracking at high particle image densities. Experiments in Fluids 57:1–27

Data Assimilation

Workshop on Optical Metrology and Data Assimilation Applied to Aeroelastics
Sept. 22-23, 2021 | TU Delft, NL & Online

Coupling experimental and computational techniques using open-source tools for FSI studies

L. Chatellier[1*], *F. Salmon*[1], *H. Bonnard*[1]
[1]Institut PPrime, UPR 3346, CNRS-Université de Poitiers-ENSMA, France
[*] ludovic.chatellier@univ-poitiers.fr

Abstract

Both experimental and numerical studies of fluid-structure interaction (FSI) problems remain challenging due to the numerical cost of multi-physics computational framework and the complexity in obtaining coupled experimental diagnostics over a complete physical system. In addition, achieving the correspondence between the numerical and experimental frameworks is not systematically guaranteed. In the solid mechanics community, model identification and FEM updating, for example, are long dating active subjects dedicated to couple numerical and experimental tools for material and structural studies. More recently, coupling, hybridation and data assimilation, among other approaches, have gained attention in the fluid mechanics community. In the context of aeroelasticity and fluid-structure interactions, modifications of existing – reliable – open-source computational tools can be viewed as a promising direction to follow. Considering that, for structure and materials exhibiting relatively simple physical behaviours, CFD is the most sensitive and numerically costly part of high Reynolds number FSI studies, it is proposed to integrate fluid and solid experimental diagnostics within open-source fluid solvers coupled with solid solvers.

The chosen framework for computational FSI studies is initially provided by the open-source coupling library preCICE (Bungartz et. al, 2016), that proposes a panel of algorithms adapted to a variety of multi-physics problems to be addressed with either open-source or proprietary codes. For the solid computational part, the open-source code Calculix (Dhondt & Wittig, 1998). On the fluid side, the finite volumes library suite OpenFOAM (Weller & Tabor, 1998) is selected for its robustness, wide range of solvers and large modularity. Additional meshing tools of the OpenFOAM suite and the Gmsh open-source mesher (Geuzaine & Remacle, 2009) are used to help handle the communication between the fluid and solid computational grids. Both the fluid and solid data couplings are performed within the OpenFOAM solvers and utilities. An application to the study of cantilevered wings at moderate Reynolds numbers is proposed (Figure 1).

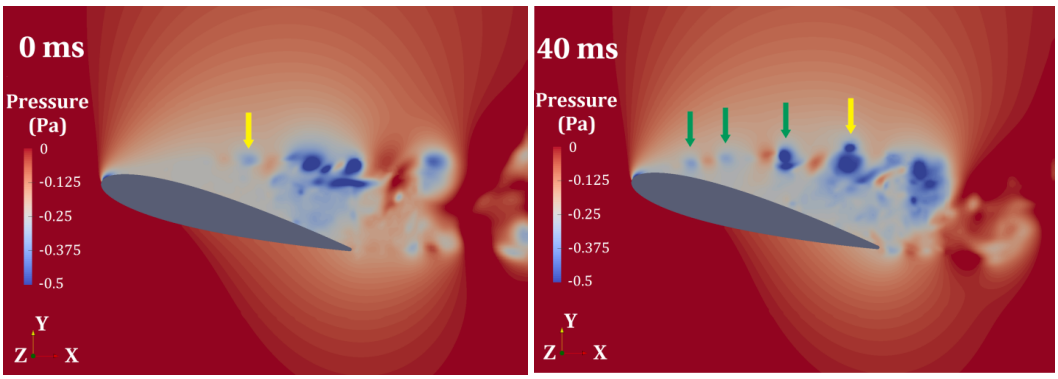

Figure 1: Pressure field computed around a deformable wing at $Re=10^5$ $M=1.8$ and $Ca=7.10^{-3}$ prior (left) and during (right) the establishment of fluid-structure interactions (Salmon & Chatellier, 2021)

Acknowledgements

This project has received funding from the European Union's Horizon 2020 research and innovation programme under grant agreement No 769237 HOMER.

References

Bungartz HJ, Lindner F, Gatzhammer B, Mehl M, Scheufele K, Shukaev A, Uekermann B, preCICE - A fully parallel library for multi-physics surface coupling, Computers & Fluids, 141, 250-258, 2016

Dhondt G, Wittig, K, CalculiX: A Free Software Three-Dimensional Structural Finite Element Program, http://www.calculix.de/, 1998

Geuzaine C, Remacle JF, Gmsh: a three-dimensional finite element mesh generator with built-in pre- and post-processing facilities, International Journal for Numerical Methods in Engineering, 79(11), 1309-1331, 2009

Salmon F, Chatellier L, 3D fluid-structure interaction simulation of an hydrofoil at low Reynolds number, *submitted to J. Fluids Struct.*, 2021

Weller HG, Tabor G, A tensorial approach to computational continuum mechanics using object-oriented techniques, Computers in Physics 12 :620, 1998

On the Development of Non-Intrusive Experimental Methods for the Nonlinear Aeroelastic Characterization of Flexible Wings

C. Mertens[*], *A. Sciacchitano*, *J. Sodja*, *B. W. van Oudheusden*
Faculty of Aerospace Engineering, Delft University of Technology, The Netherlands

[*]C.Mertens@tudelft.nl

Motivation

As a result of the efforts to reduce the structural weight and increase the aerodynamic efficiency of aircraft on all scales, lighter and more flexible fixed-wing structures are built that exhibit larger levels of deformation under aerodynamic load. These deformations can become so large that nonlinear aeroelastic effects occur (see Dimitriadis, [1]). Current numerical models for aeroelastic predictions can account for these effects only to a limited extend, as aeroelastic prediction models are typically reduced-order models. The inclusion of nonlinear effects in these models is a topic of ongoing research, and the development of these novel nonlinear aeroelastic prediction models needs to be supported with experimental validation data, which can be generated in wind tunnel experiments.

The instrumentation of flexible wing structures with different sensors to perform a complete aeroelastic characterization in terms of the three forces in Collar's triangle (aerodynamic, inertial, elastic) is unfeasible. A possible alternative is to perform optical measurements of the flow field and the structural motion using Lagrangian Particle Tracking (LPT) and determine the forces based on these measurements. The complete aeroelastic characterization can then be performed using different physical models for the flow and for the structure, that relate the flow field and the structural motion to the aerodynamic and structural forces, respectively.

Integrated Measurement Approach

A series of wind tunnel measurements has been conducted in the Aerodynamics Laboratories of TU Delft considering both a rigid pitching wing and a flexible wing subject to periodic and unsteady gusts. Non-intrusive measurements of the flow field and the structural motion of moving and/or deforming wings can be performed with the integrated approach described in Mertens et al. [2]. In this approach, combined optical measurements of structural markers and flow tracer particles are acquired and separately processed with the LPT algorithm Shake-The-Box. The LPT position measurements of the structural markers are used to determine the shape and position of the moving and deforming wing, as shown in Figure 1 together with the LPT-based measurement of the phase-averaged unsteady flow velocity field at four different phase instants.

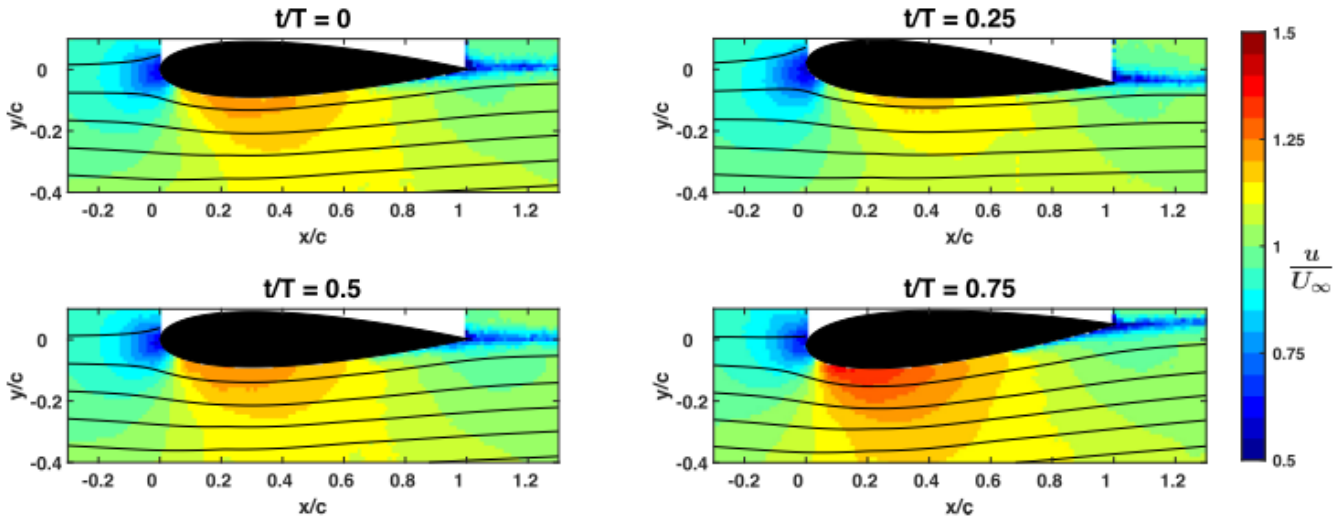

Figure 1: LPT-based measurement of the unsteady flow field and position of a pitching wing [2]

Aeroelastic Characterization of Flexible Wings

When the measurements of the flow field and the structural motion of a flexible wing are obtained with the integrated approach, these data can be used together with physical models to determine the forces that act on the flexible wing during the aeroelastic interaction. In the linear aeroelastic regime of relatively small deformations and mostly attached flow, physical models of relatively low complexity provide satisfactory results. In Figure 2, the three forces of the aeroelastic interaction on a flexible wing in unsteady periodic inflow, as well as the measurement residual δ, are shown, where an unsteady potential flow model was used to determine the aerodynamic force from the flow field measurements and an Euler-Bernoulli beam model was used to determine the inertial and elastic forces from the structural markers.

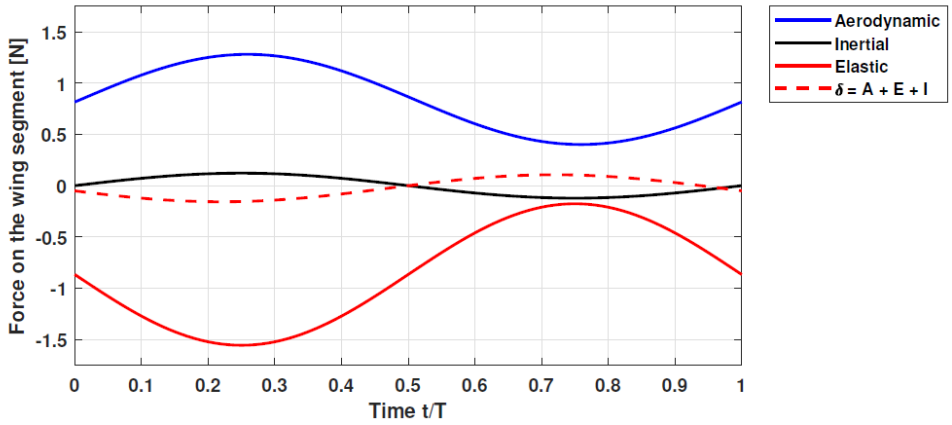

Figure 2: Collar's triangle of forces acting on a flexible wing as determined from the LPT measurements [3]

Outlook to Future Work

After demonstrating the experimental determination of the unsteady flow field and the structural motion of moving and deforming wings with an integrated measurement approach, as well as the determination of the forces that characterize the aeroelastic interaction in the linear regime, the next step is to extend the experimental analysis using non-intrusive methods to the nonlinear aeroelastic regime. This research activity is performed by investigating the highly flexible benchmark wing that was introduced in 2021 by Avin et al. [4] with the integrated measurement approach. This highly flexible wing can sustain wingtip deformations of up to 50% of the span, which is large enough to enter the nonlinear aeroelastic regime. The analysis methods for the experimental data have to be adjusted to the occurrence of these effects, before the results can be compared to numerical model data in validation activities.

Acknowledgements

This project has received funding from the European Union's Horizon 2020 research and innovation programme under grant agreement No 769237 HOMER.

References

[1] G. Dimitriadis, "Introduction to Nonlinear Aeroelasticity," John Wiley and Sons, 2017.
[2] C. Mertens, A. Sciacchitano, B. W. van Oudheusden, J. Sodja, "An integrated measurement approach for the determination of the aerodynamic loads and structural motion for unsteady airfoils," Journal of Fluids and Structures 103, 2021.
[3] C. Mertens, T. de Rojas Cordero, J. Sodja, A. Sciacchitano, B. W. van Oudheusden, "Determination of Collar's Triangle of Forces on a Flexible Wing Based on Particle Tracking Velocimetry Measurements," AIAA SciTech Forum, 2021.
[4] O. Avin, D. E. Raveh, A. Drachinsky, Y. Ben-Shmuel, M. Tur, "An Experimental Benchmark of a Very Flexible Wing," AIAA SciTech Forum, 2021.